Metal decorated carbon nanotubes for electrocatalytic water splitting

Luca Cozzarini [a,*], *Gabriele Bertolini* [b], *Simone Tommaso Šuran-Brunelli* [a], *Andrea Radivo* [a], *Maria Victoria Bracamonte* [c], *Claudio Tavagnacco* [c], *Andrea Goldoni* [a,**]

[a] *Elettra Sincrotrone Trieste, S.S. 14 - Km 163.5 in Area Science Park, 34149, Trieste, Italy*
[b] *Laboratory for Solid State Physics, ETH Zurich, Zurich, 8093 Switzerland*
[c] *Department of Chemical and Pharmaceutical Sciences and INSTM UdR Trieste, University of Trieste, Via L. Giorgieri 1, 34127, Trieste, Italy*

ARTICLE INFO

Article history:
Received 23 December 2016
Received in revised form
5 June 2017
Accepted 13 June 2017
Available online 5 July 2017

Keywords:
Water electrolysis
Carbon nanotubes
Catalyst
Hydrogen production

ABSTRACT

Water is the most abundant, renewable source of hydrogen on our planet. Appropriate catalytic materials are needed to minimize the energy required to electrochemically split the water molecule, and electrode with high specific areas are sought to maximize the electrolyte/electrode interface. We use Carbon Nanotubes (CNTs) bundles as templates for water splitting electrodes fabrication. Appropriate catalyst materials are thermally evaporated on CNTs, to exploit both their good electrical conductivity and large specific area, while optimizing over-potential towards Hydrogen Evolving Reaction (HER) or Oxygen Evolving Reaction (OER) through the deposited catalysts. Electrodes morphology and surface chemistry are characterized, before and after electrolysis, by means of scanning electron microscopy and X-ray photoelectron spectroscopy. Our electrodes are able to perform water oxidation and water reduction near their thermodynamical limit. Performances of these electrodes, taking into account the extremely low loading mass of catalytic material (10^{-2} mg cm^{-2}) with respect to other reported systems, are among the best HER and OER system reported so far. Finally, a working electrolyser, capable to operate at the interesting low voltage of a single AA battery (1.5 V) and output a stable current (>2.0 mA cm^{-2}) for at least 20 h, is successfully assembled and tested.

Introduction

A valid method to obtain high-purity hydrogen is to split water into hydrogen and oxygen through an electrolyser. In practice, this process is hampered by the high amount of energy required for the overall reaction $2H_2O \rightarrow 2H_2 + O_2$ ($\Delta G = 237.21$ kJ mol^{-1}, in standard conditions), giving a minimum theoretical decomposition voltage $E_o = 1.23$ V, to be applied to the electrolyser just to start water splitting [1–3]. As

* Corresponding author.
** Corresponding author.
E-mail addresses: luca.cozzarini@elettra.eu (L. Cozzarini), andrea.goldoni@elettra.eu (A. Goldoni).
http://dx.doi.org/10.1016/j.ijhydene.2017.06.101

a matter of fact, a greater voltage is usually required, due to the over-potentials associated to the cathode and anode reactions, forcing commercial water electrolysers to operate at voltages above 1.8–2.0 V (overall over-potential > 650 mV) [1,4–6]. To optimize electrolyser efficiencies, the main effort is to achieve useful current densities at the lowest possible over-potential.

Greatest known catalytic material for cathode water reduction is Pt, that shows the lowest over-potential towards Hydrogen Evolution Reaction (HER) [4,7], while the RuO_2 and IrO_2 are the ideal choices for anodic water oxidation (Oxygen Evolution Reaction – OER) [5,7]. The high cost and rarity of these noble metals represent an obstacle to their large-scale use in electrolysis devices. In recent years, efforts have been made to use earth-abundant materials such as transition metals and their oxide as catalysts [6]. In particular, Co oxide nano-particles [5], Co oxide/graphite nano-composites [8] and Ni borate films [9] have been successfully tested as OER catalysts; Ni/NiO nano-particles as HER catalysts [10], while mixed transition metal oxide nano-particles showed good performance both in OER and HER [11]. Moreover, Pd has been taken into consideration since it shows a catalytic activity similar to Pt [12–15], while being available at a price ranging between 40% and 60% of Pt in the last 5 years [16]. In parallel with electrode material choice, an essential aspect to improve electrolyser efficiency is to maximize the catalyst surface exposed to the electrolyte and to minimize the current density and amount of material used [17,18]. This objective is usually achieved by fabricating high specific area electrodes, both by dispersing catalyst materials on high porosity conductive supports or fabricating the catalysts themselves in the form of highly porous films [18–20]. In this work we selected Carbon Nanotubes (CNTs) as conductive templates for water splitting electrodes. While in general carbon surfaces show low chemical reactivity towards HER and OER, one big advantage of using CNTs as electrochemical support are their good electrical conductivity and large specific area, which can greatly increase the contact surface between the reactants [17,21–23]. Several approaches were tried in order to enhance CNT catalytic properties decorating their surface with either thin layers or nano-particles of appropriate inorganic material [17,24]. Reported methods are generally divided into three categories [22,25]: (1) *filling* (placing chemical species inside CNT channels); (2) *ex-situ* (pre-formed inorganic particles attached to CNTs *via* chemical interactions); (3) *in-situ* (inorganic components are synthesized on pristine or functionalized CNTs). Few works reported so far on the decoration of CNTs with metals and metal oxides through atomic layer deposition or thermal evaporation [21,26–29]. The approach proposed in this work is to decorate the CNTs with catalyst layers using the latter, simple physical method. In this way, we are able to evaporate a thin layer of the appropriate metal to exploit both the high surface area of CNTs, increasing the catalyst surface interfaces, while optimizing over-potential towards HER or OER through the catalytic deposited layer. We show that, in certain cases, this allows electrodes to perform water oxidation at over-potential as low as 200 mV and water reduction near its thermo-dynamical limit.

Experimental

Electrodes fabrication

Multi-walled carbon nanotubes (CNTs) were grown by chemical vapour deposition on native SiO_2 on Si wafers (SiO_2/Si) where a thin layer of growth catalyst (Fe, ≈ 3 nm) was previously evaporated. Wafers were cut into 10 × 5 mm pieces prior to CNT growth. Hydrogen and acetylene were used as reduction and synthesis gases, respectively. Wafer surface temperature was set to 670 °C for reduction (H_2 pressure: 10 Pa for 5 min) and 730 °C for CNT synthesis (C_2H_2 pressure: 5×10^3 Pa for 5 min); heating ramp was set to 70 K min^{-1}. Wafers with grown CNTs (named "pristine CNTs") were cooled in vacuum (10^{-3} Pa), then stored in standard atmosphere. Metals (Pd 99.99%, Ni 99.98%, Co 99.95% - all purchased from Advent Research Materials) were thermally evaporated in vacuum (10^{-3} Pa) on pristine CNT samples. Evaporator shutter opening time varied from 150 to 300 s, to obtain a metals loading on CNTs of about 8×10^{-2} mg cm^{-2}. Evaporation deposition rates (5.5×10^{-4} mg s^{-1} cm^{-2} for Pd, 2.3×10^{-4} mg s^{-1} cm^{-2} for Co, 3.1×10^{-4} mg s^{-1} cm^{-2} for Ni) were previously estimated by evaporating in the same conditions Pd, Co or Ni layers on a glass slides for different times, then measuring their thickness through Atomic Force Microscopy (AFM). Deposited masses were obtained after multiplying the volume (measured thickness x sample surface) by the density of Pd, Co or Ni. Evaporation rates were then linearly extrapolated from these data. Estimated sample loading was consistent with average volume increase of CNTs after metal evaporation (considering cylindrical nanotubes with an average length of 10 μm and a density of 5×10^8 nanotubes cm^{-2}). The volume increase was estimated from average thickness comparison of Scanning Electron Microscopy (SEM) images of CNTs before and after metal evaporation. Samples were cooled in vacuum and then stored in standard atmosphere conditions. Samples were named as "CNTs/metal", where "metal" is the evaporated element (Co, Ni or Pd). Before electrochemical measurements, one edge of the sample was covered with conductive silver paste; half of the electrode was masked using an electrically insulating polymer to expose 5 × 5 mm of geometric electrode area. This exposed a geometric area that was used for subsequent current density normalizations. Analogous samples using graphite instead of CNTs were also fabricated. Graphite conductive paint (Graphit 33, Kontact Chemie) was applied on 10 × 5 mm Si wafers (SiO_2/Si), then Pd, Ni or Co were evaporated in the same condition of CNT samples. Before electrochemical measurements, one edge of the sample was covered with conductive silver paste; half of the electrode was masked using an electrically insulating polymer to expose 5 × 5 mm of geometric electrode area.

Scanning electron microscopy and atomic force microscopy

Scanning Electron Microscopy (SEM) image of electrodes were acquired using a Zeiss Supra40, at 20 kV accelerating voltage. Atomic Force Microscopy (AFM) was a XE-100 (Park-Systems), used in contact mode with Silicon tips (CSC 36/no Al,

MikroMasch, USA); a typical force constant of 0.6 N m^{-1} was employed.

X-ray photoelectron spectroscopy

XPS was carried out on a modified ultra-high-vacuum VG Escalab II spectrometer. Non-monochromatized Al Kα exciting X-ray radiation (1486.6 eV, 225 W) was used. Possible binding energy correction due to sample charging was applied by assuming the C1s core level line at 284.5 eV. The background of the spectra was subtracted using a Shirley integrating algorithm. The core level peaks were fitted using Voigt functions.

Electrochemical measurements

Linear sweep voltammograms (LSV) were performed on a Autolab 302 N electrochemical workstation (Metrohm, The Netherlands) at room temperature, using a conventional three-electrode system composed of a platinum wire as an auxiliary electrode and a Ag/AgCl (3 M NaCl) (CH Instrument, CH 111) as a reference electrode. Potassium phosphate buffer solution (PBS; pH 7; 0.1 M) was use as supporting electrolyte and the scan rate was 0.02 V s^{-1}. All reported potentials were converted to reversible hydrogen electrode according to: $E_{RHE} = E_{Ag/AgCl} + 0.197 + 0.059$ pH. Overall water-splitting measurements were carried out in a custom two-electrode system. 0.1 M PBS (pH 7) was used as supporting electrolyte. For benchmark reference, a Ni foil was used as anode (positive electrode for OER) and a Pt foil as cathode (negative electrode for HER). Then, pristine CNTs, CNTs/Co and CNTs/Ni were tested as anodes (cathode: Pt foil). Pristine CNTs and CNTs/Pd where tested as cathodes (anode: Ni foil). Finally, also the CNTs/Co as anode and CNTs/Pd as cathode were used. A Keithley 2400 multimeter controlled by a National Instruments Labview VI was used as power supply and data log. All of the above water splitting configurations were tested by (a) registering the current as a function of applied potential (linear sweep voltammetry, from 0.00 to 2.50 V, scan rate 0.05 V s^{-1}) and (b) registering the current as a function of time (0–120 s) in controlled potential electrolysis method (at 1.00 V, 1.25 V, 1.50 V, 1.75 V and 2.00 V). The best performing configuration, the CNTs/Co as anode and the CNTs/Pd as cathode, was also tested at 1.50 and 2.00 V for longer times (20 h).

Results and discussion

CNTs/metal electrodes fabrication

Electrodes (schematized in Fig. 1, left) were successfully assembled as explained in Section Electrodes fabrication. A picture of a typical electrode is shown in Fig. 1, right.

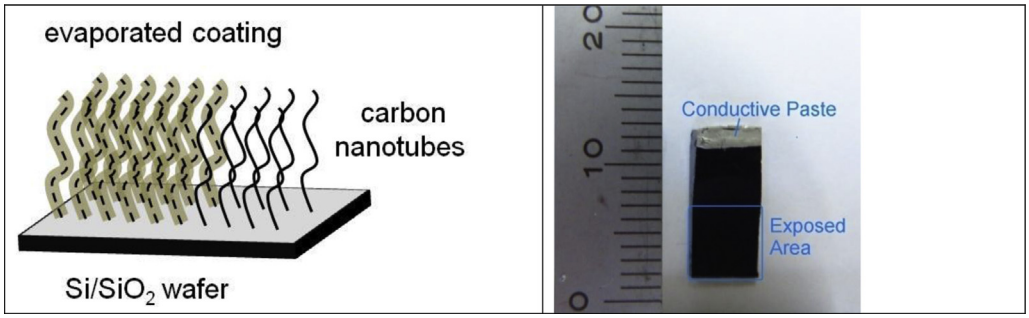

Fig. 1 – (left) schematic illustration of CNT/metal electrode; (right) photo of a final electrode. Ruler scalebar is in mm.

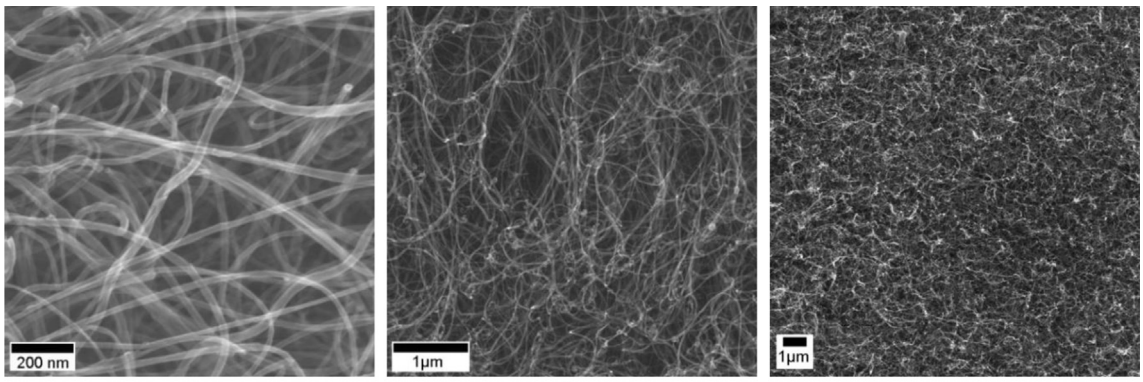

Fig. 2 – SEM images of Pristine CNTs at (a) 200 K, (b) 50 K, (c) 15 K magnification.

Morphology of CNTs/metal nanostructures

Average diameter of pristine CNTs (determined from SEM images – Fig. 2 a–c) is 23 ± 3 nm. After evaporation, SEM images (Fig. 3 a–c; Fig. 4 a–c; Fig. 5 a–c) show a uniform coating of the nanotubes. CNTs/Co, CNTs/Ni and CNTs/Pd diameters increased by a factor 1.5–1.7. This value agrees with the expected deposition trend (the higher the amount of deposited metal, the higher the diameter of the samples). Deposition times, estimated catalyst loading and diameters are reported in Table 1.

Chemical nature of CNTs/metal nanostructures

XPS positively identified Pd, Ni and Co core lines on CNTs/Pd, CNTs/Ni and CNTs/Co, respectively. Fig. 6a shows the XPS spectra of the CNTs/Pd, where two well define peaks at 335.0 eV and 340.5 eV are observed, corresponding the

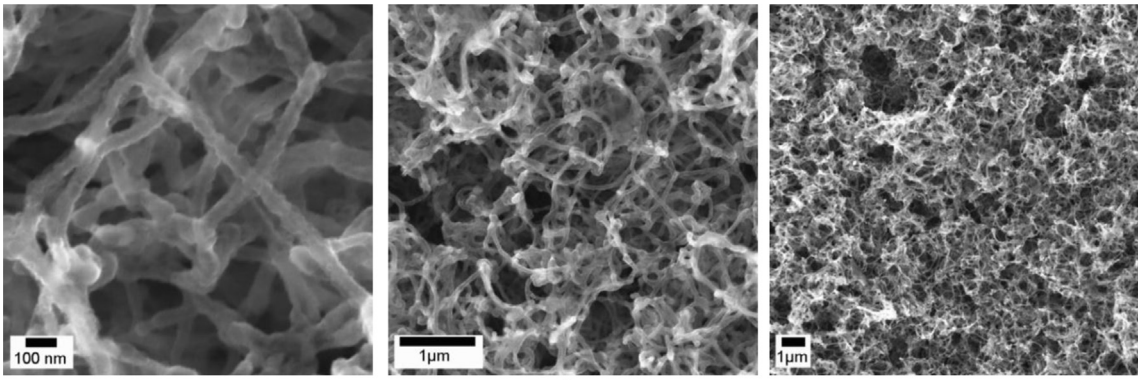

Fig. 3 – SEM images of: CNT/Co at (a) 200 K, (b) 50 K, (c) 15 K magnification.

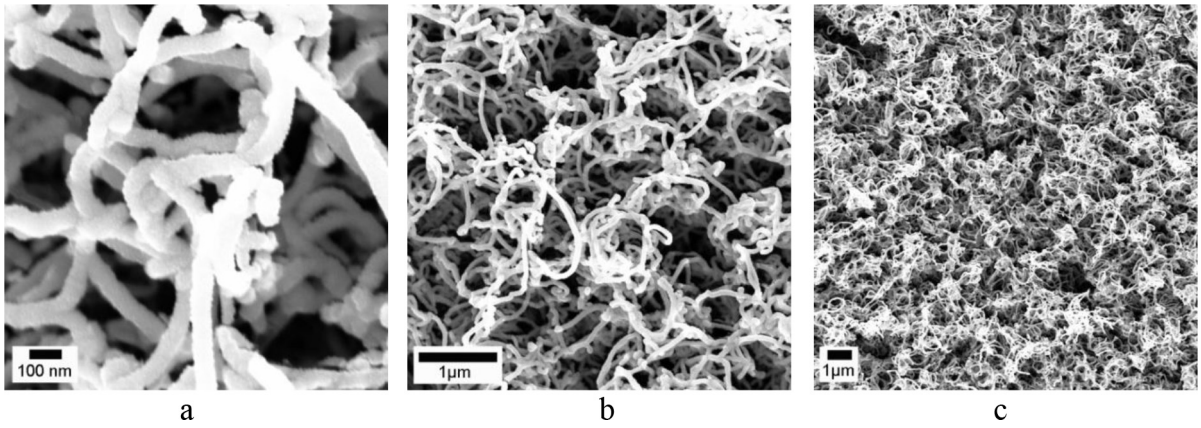

Fig. 4 – SEM images of: CNT/Ni at (a) 200 K, (b) 50 K, (c) 15 K magnification.

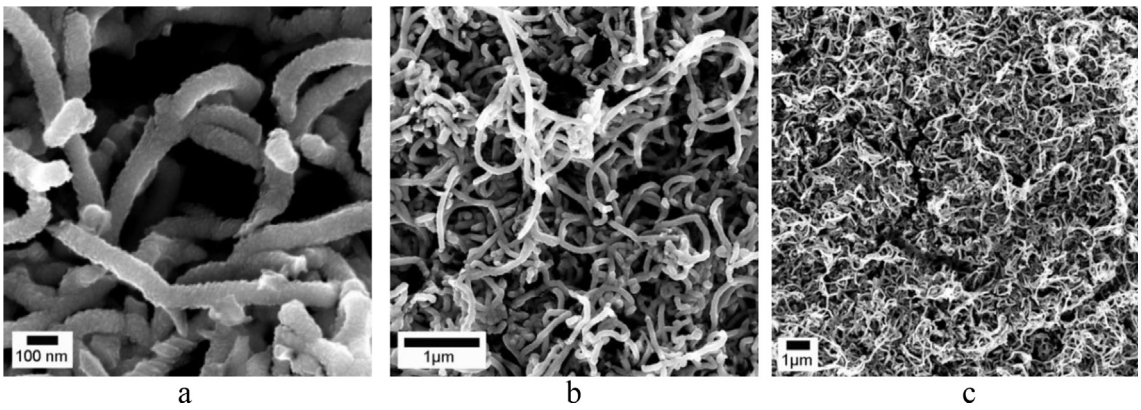

Fig. 5 – SEM images of: CNT/Pd at (a) 200 K, (b) 50 K, (c) 15 K magnification.

Table 1 – Measured average diameters of CNTs and CNTs/metal nanostructures; evaporation time and estimated catalyst loading.

Sample	Avg. diameter [nm]	Evaporation time [s]	Estimated catalyst loading [mg cm^{-2}]
Pristine CNTs	23 ± 3	–	–
CNTs/Co	60 ± 9	300	(7.0 ± 1.0) $\times 10^{-2}$
CNTs/Ni	64 ± 6	300	(9.0 ± 1.0) $\times 10^{-2}$
CNTs/Pd	77 ± 5	150	(8.0 ± 1.0) $\times 10^{-2}$

characteristic metallic Pd features [30–32]. XPS spectra of CNTs/Co (Fig. 6b, red curve) show two peaks in the Co2p3/2 region (778.0 eV and 780.5 eV) and a satellite feature (785.0 eV). First peak was identified as signature of metallic Co [33,34]. The second peak (780.5 eV), due to the presence of the satellite where is distinctive feature of Co(II) [33,34], was assigned to Co(II) oxide. Similarly, CNTs/Ni XPS spectrum (Fig. 6c) shows two peaks (852.4 eV and 855.0 eV) plus a satellite structure (860.5 eV), in the Ni2p3/2 region. Peaks were identified as signature of metallic Ni and Ni(II) oxide respectively [33,35]. In the case of evaporation of Co and Ni on CNTs, an oxidation of the metallic coating in atmosphere seems to take place.

Effect of CNTs, CNTs/Co and CNTs/Ni as OER catalysts

The oxidation voltammograms between 0.80 V and 1.80 V of CNTs, CNTs/Co, CNTs/Ni and their corresponding analogous using graphite as support is shown in Fig. 7. No significant response is observed in the case of graphite supports. For the CNTs samples, the performance of the materials was analyzed comparing the current densities at a fixed over potential ($\eta = 0.50$ V). The obtained values were 2.00 mA cm^{-2} and 0.30 mA/cm^{-2} for CNTs/Co and CNTs/Ni, respectively, indicating that higher activity in the case of Co-decorated samples. Current registered below $\eta = 0.50$ in CNT/Co is most probably related to the catalyst oxidation. Pristine CNTs do not show any appreciable current output at the same over-

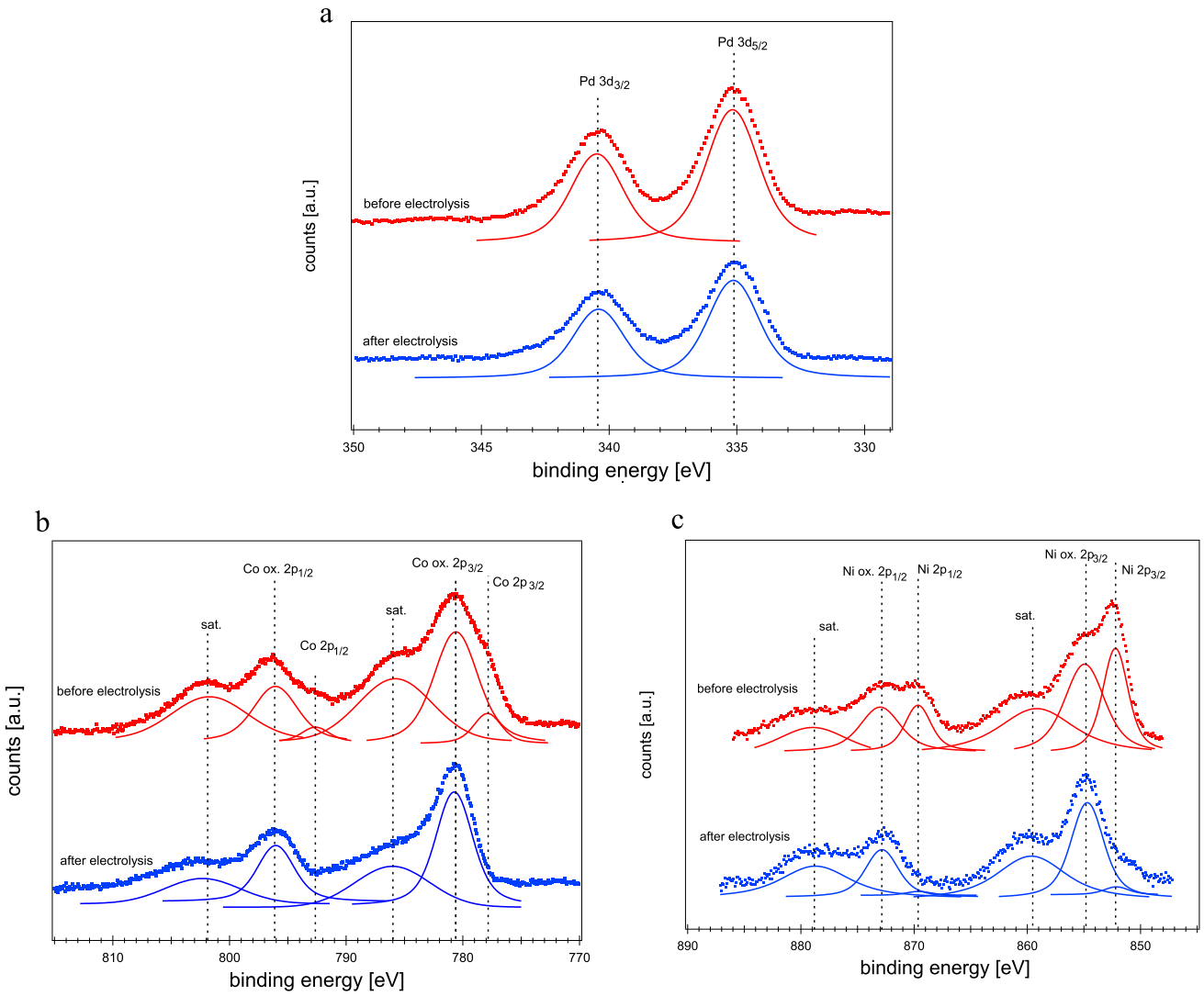

Fig. 6 – XPS spectra (dotted) and fitting peaks (continuous lines) of: (a) 3d region of CNT/Pd; (b) 2p region of CNT/Co; (c) 2p region of CNT/Ni; before (red) and after (blue) electrochemical measurements. (For interpretation of the references to colour in this figure legend, the reader is referred to the web version of this article.)

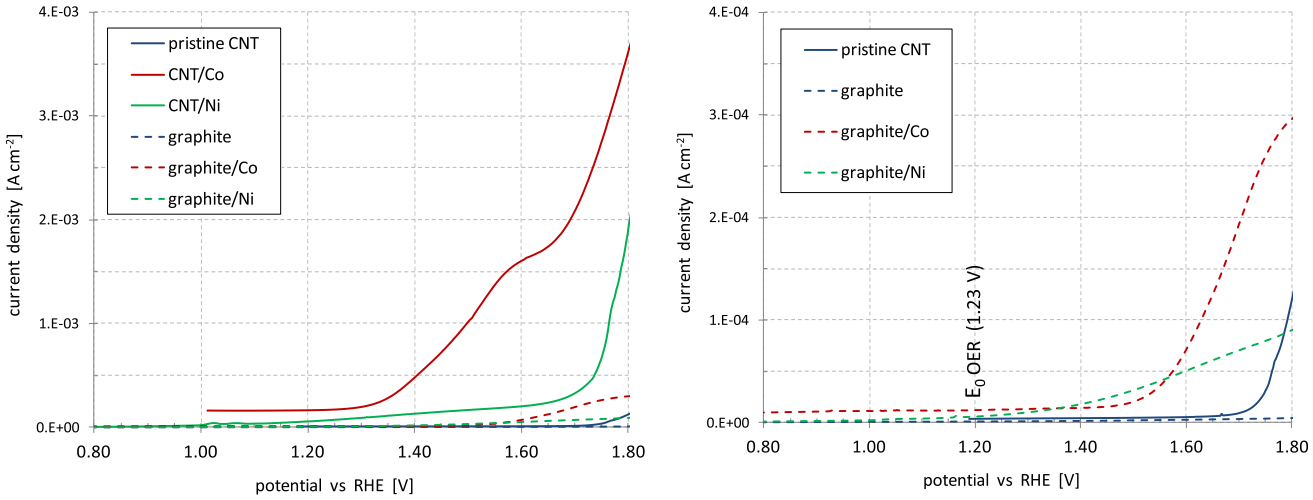

Fig. 7 – (left) Voltammograms (in oxidation) of CNT/Ni (continuous curve, green) and CNT/Co (red) compared to pristine CNT (in blue), graphite (dotted blue), Ni on graphite (dotted green) and Co on graphite (dotted red) are shown. (right) Voltammograms of graphite and catalyst on graphite, compared to pristine CNT, are shown more in details with rescaled y-axis. (For interpretation of the references to colour in this figure legend, the reader is referred to the web version of this article.)

potential. Further analysis were performed comparing the over potential (determined form the onset potential) for each sample. In case of CNTs/Co the over potential is around 0.20–0.30 V, while for CNTs/Ni is 0.50 V. These data show promising catalytic activities of Co oxide on CNTs towards OER.

Effect of CNTs, CNTs/Pd, CNTs/Co and CNTs/Ni as HER catalysts

Reduction voltammogram (between 0.50 V and −1.00 V) of CNTs, CNTs/Pd, CNTs/Co and CNTs/Ni and their corresponding analogous using graphite as support is shown in Fig. 8. Also in this case, no significant response is observed for of graphite supports. For the CNTs/metal samples, the performance of the materials was analyzed comparing the current densities at a fixed over potential (η = 0.35 V). The obtained values were 3.0 mA cm^{-2}, 1.5 mA cm^{-2} and 1.0 mA cm^{-2} for CNTs/Pd, CNTs/Co and CNTs/Ni, respectively, indicating that higher activity in the case of Pd-decorated samples. Pristine CNTs do not show any appreciable current output at the same over-potential, while Pd on graphite outputs only 0.5 mA cm^{-2}. Further analysis were performed comparing the over potential (determined from the onset potential) for each sample. In case of CNTs/Co

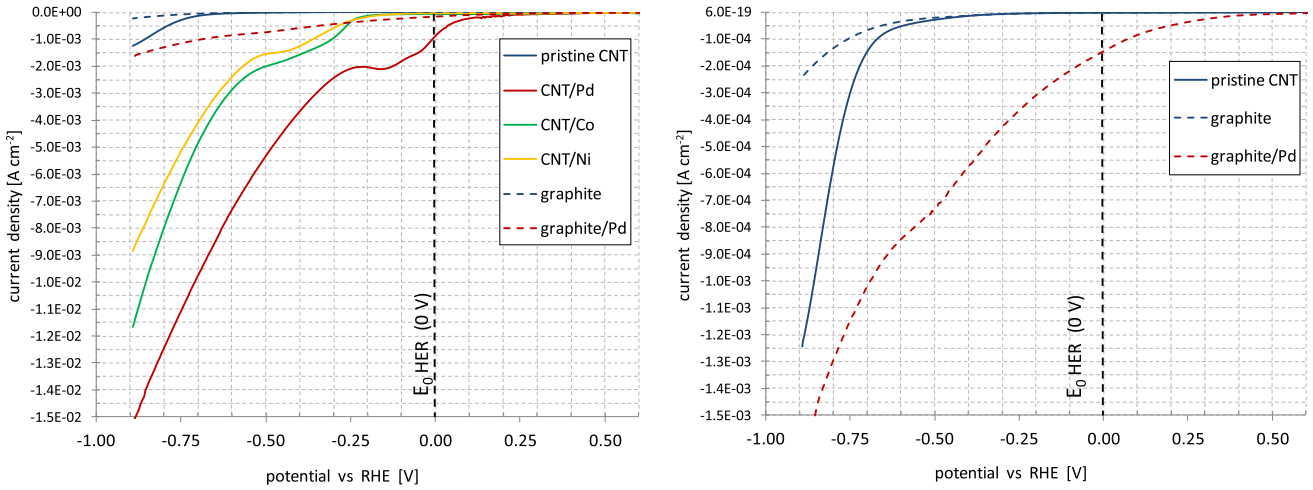

Fig. 8 – (left) Voltammograms (in reduction) of CNT/Ni (continuous curve, yellow), CNT/Co (green), CNT/Pd (red) compared to pristine CNT (blue), graphite (dotted blue) and Pd on graphite (dotted red) are shown. (right) Voltammograms of graphite, Pd on graphite and pristine CNT, are shown more in details with rescaled y-axis. (For interpretation of the references to colour in this figure legend, the reader is referred to the web version of this article.)

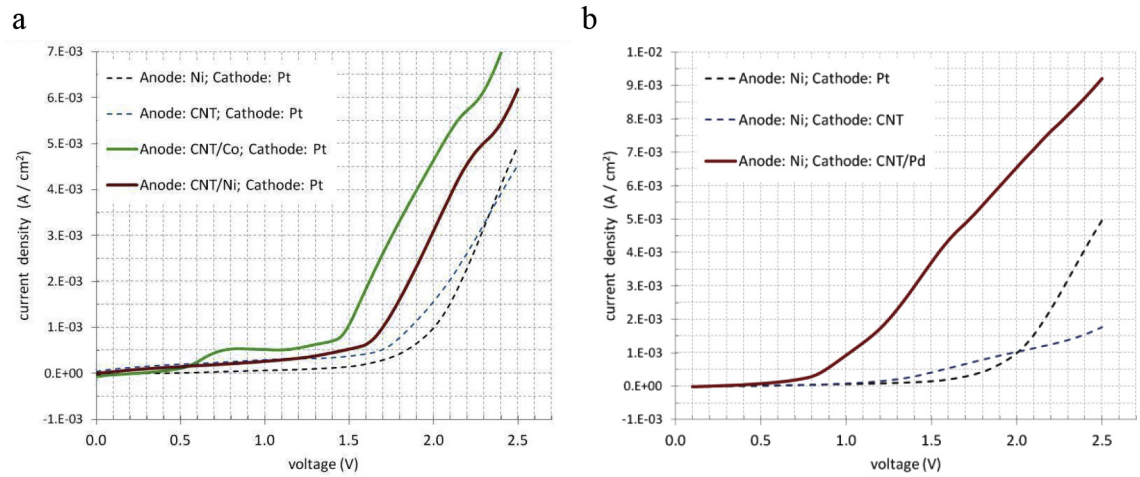

Fig. 9 – (a) Voltammetry of water electrolysis process using a standard cathode (Pt foil), while testing different anodes at low catalyst loading: pristine CNT (dotted blue curve), CNT/Ni (red), CNT/Co (green). Reference cell electrolysis, with benchmark anode (Ni foil) and cathode (Pt foil) is reported for comparison (dotted black); (b) voltammetry of water electrolysis process using a standard anode (Ni foil), while testing different cathodes: pristine CNT (dotted blue curve) and CNT/Pd (red) at low catalyst loading. Reference cell electrolysis (Ni foil/Pt foil) is reported for comparison (dotted black). (For interpretation of the references to colour in this figure legend, the reader is referred to the web version of this article.)

and CNTs/Ni the over potential is around 0.25 V, while for CNTs/Pd it seems near to zero. In this particular case, current registered below $\eta = 0$ is most likely related to H_2 adsorption on Pd and PdH_X formations [36,37]. Hydrogen evolution can be noticed by direct observation (bubbles) starting around $\eta = 0.15–0.20$ V. These data suggest very interesting catalytic activities of Pd deposited on CNTs towards HER; also Ni oxide and Co oxide show promising properties.

Electrolysis

Overall, the water splitting experiments comply with linear sweep voltammetry data trends. Reference cell (anode: Ni foil; cathode: Pt foil) requires a minimum applied voltage of about 1.70 V to start electrolysis process (Fig. 9 a–b, black dotted curve); at 2.00 V and 2.50 V it outputs about 1.00 mA cm^{-2} and 5.00 mA cm^{-2}, respectively. Pristine CNTs seem to behave similarly with respect to the reference at any applied potential if used as anode (Fig. 9 a-blue dotted curve), worst if used as cathode (Fig. 9 b - blue dotted curve). Testing CNTs/Co as anode (Fig. 9 a, green curve) allows to starting electrolysis at lower potential (1.50 V) and increases greatly the current density at 1.75 V (3.00 mA cm^{-2} *vs* 0.50 mA cm^{-2}) with respect to the reference cell. CNTs/Ni samples (Fig. 9 a – red curve) show a similar behaviour (electrolysis starts at 1.60 V; 2.00 mA cm^{-2} at 1.75 V). In fixed potential experiments (continuous electrolysis for 2 min – see Fig. 10), no difference can be appreciated with respect to the reference cell (Fig. 10 a), if a 2.00 V potential is applied. Nevertheless, the final, stabilized current density output is doubled at 1.50 V (0.25 mA cm^{-2} *vs* 0.12 mA cm^{-2}) and nearly tripled at 1.75 V (0.50 mA cm^{-2} *vs* 0.18 mA cm^{-2}) for both CNTs/Co and CNTs/Ni anodes (Fig. 10 d–e). If CNTs/Pd are tested as cathode (Fig. 9c), electrolysis starts at very low potential (bubbles can be seen just above the minimum required potential of 1.23 V; current flow registered below 1.23 V can be attributed to hydrogen adsorption/desorption into Pd [36,37], and a huge difference is noticed in respect to the benchmark Pt/Ni cell at every applied potential in sweep voltammetry (current density: 2.5 mA cm^{-2} at 1.50 V, 6.0 mA cm^{-2} at 2.00 V and nearly 10 mA cm^{-2} at 2.50 V). The difference is relevant also at fixed potentials: current density, after 2 min electrolysis, reaches stable values of 5.0 mA cm^{-2}, 3.0 mA cm^{-2} and 1.5 mA cm^{-2} at 2.00 V, 1.75 V and 1.50 V, respectively (Fig. 10f). In the final water splitting configuration (CNTs/Pd as cathode and CNTs/Co as anode – Fig. 10g) the behavior is similar to that reported for the previous system, but current density is even higher at low voltage (2.0 mA cm^{-2} after 2 min at 1.50 V). Moreover, a current of about 1.0 mA cm^{-2} can be registered after applying 1.25 V for 2 min. Current densities appear to stabilize between 60 and 75% of their original values after 20 h continuous electrolysis: registered output after these lengthier experiments are still as high as 2.2 mA cm^{-2} and 4.0 mA cm^{-2} (applying 1.50 V and 2.00 V) as shown in Fig. 11. This shows the time stability of these electrodes; remarkably, a stable output >2.0 mA cm^{-2} can be obtained at 1.50 V (i.e. the nominal voltage supplied by a single AA battery). Figs. 11 and 12.

Electrode characterization after electrochemical measurements

SEM images (Figs. 12–14) suggest a good conservation of catalyst layer after continuous electrolysis (20 h) at 2.00 V; average diameters (reported in Table 2) of CNTs/Pd and CNTs/Ni appear similar to those before the experiment; on the other hand, CNTs/Co increase their diameter. This increase (corresponding to an increment in volume between 2 and 3 times) can be due to a phase transformation from the initial Co/Co(II)

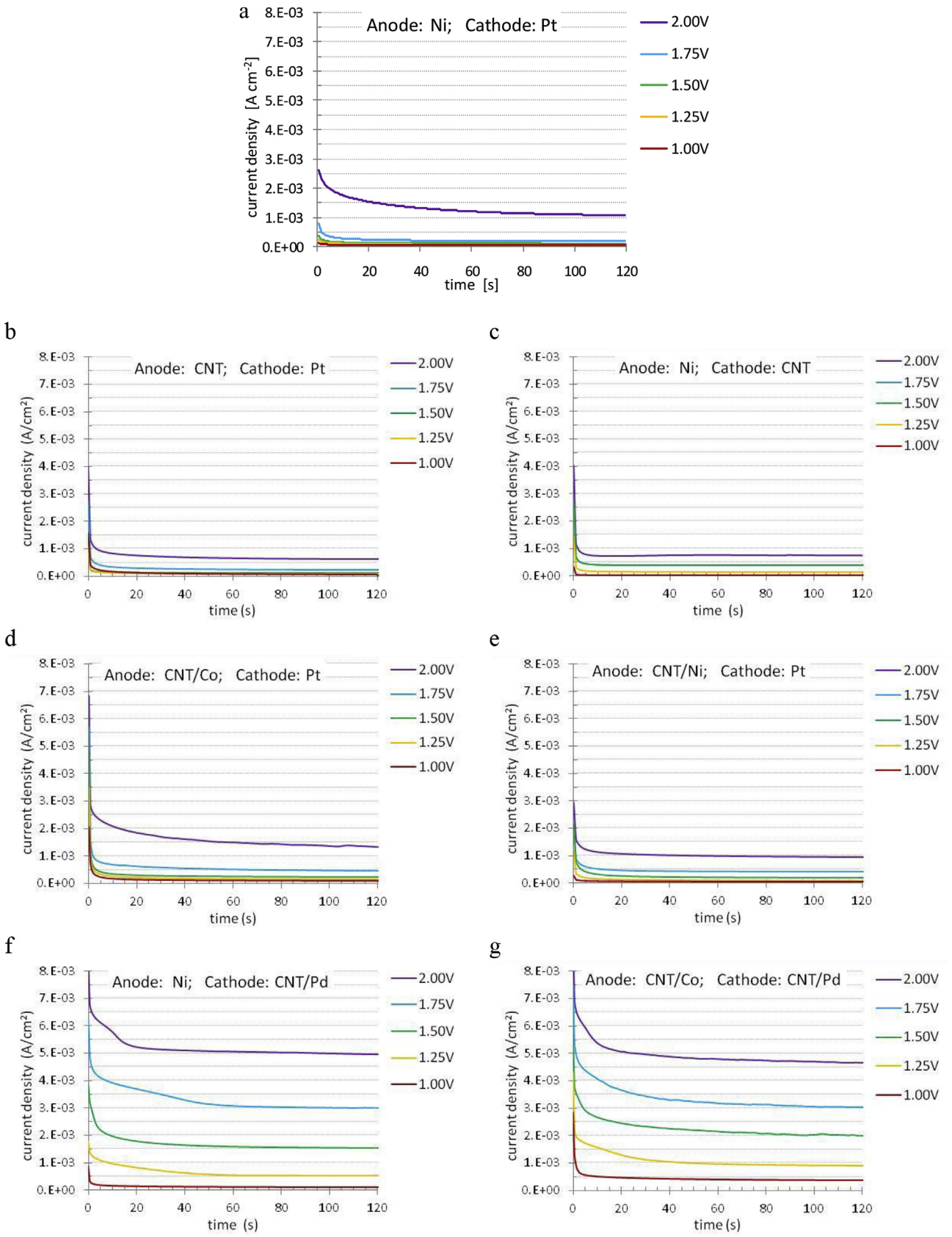

Fig. 10 – Fixed potential electrolysis for different cell configurations (A = Anode; C = Cathode) and voltages: (a) A: Ni; C: Pt (reference cell); (b) A: CNT; C: Pt; (c) A: Ni; C: CNT; (d) A: CNT/Co; C: Pt; (e) A: CNT/Ni; C: Pt; (f) A: Ni; C: CNT/Pd; (g) A: CNT/Co; C: CNT/Pd.

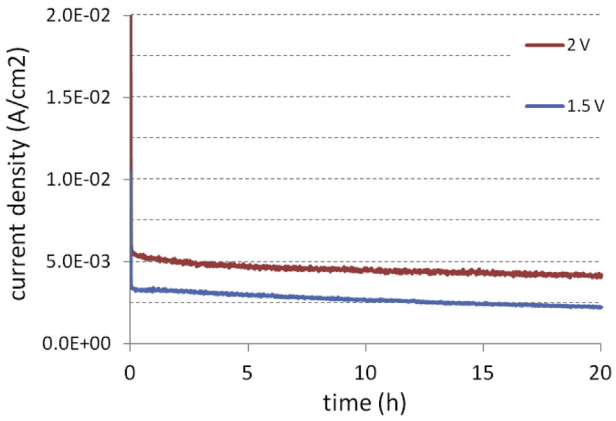

Fig. 11 – Long time (20 h) fixed potential electrolysis of best performing cell configuration (Anode: CNT/Co; Cathode: CNT/Pd).

oxide into Co(III) oxide or Co(II)/Co(III) hydroxide, as pointed out by XPS data reported in Table 3 and in Fig. 6. CNTs/Pd XPS peaks morphology/position after short and long electrolysis trials do not show any noticeable difference in respect to the spectra acquired before electrolysis (see Fig. 6a: blue curve *vs* red curve, and Table 3). Co and Ni signals are also found on respective samples after longer electrolysis. On CNTs/Co (Fig. 6b: blue curve *vs* red curve), the peak at 778.0 eV (previously identified as metallic Co) disappeared, prompting to a complete oxidation of remaining metallic Co; the second peak (780.5 eV), that can be related either to Co(II) or Co(III) oxide, is still noticeable; moreover, due to the attenuation of the satellite typical of Co(II) [33,34], that was clearly seen in XPS spectra before the electrolysis, a partial transformation of Co(II) oxide into Co(III) oxide during electrolysis can be conceived (ratio between oxide to satellite signal was 1.2 before electrolysis, 1.6 after). On CNTs/Ni (Fig. 6c: blue curve *vs*

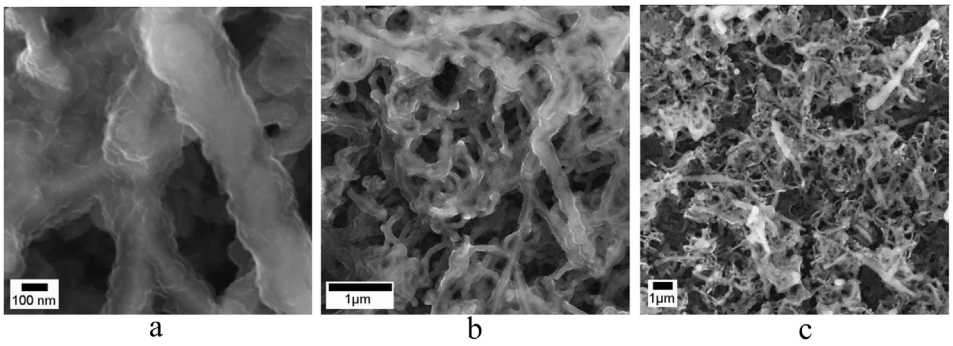

Fig. 12 – SEM images of CNT/Co after electrolysis at (a) 200 K, (b) 50 K, (c) 15 K magnification.

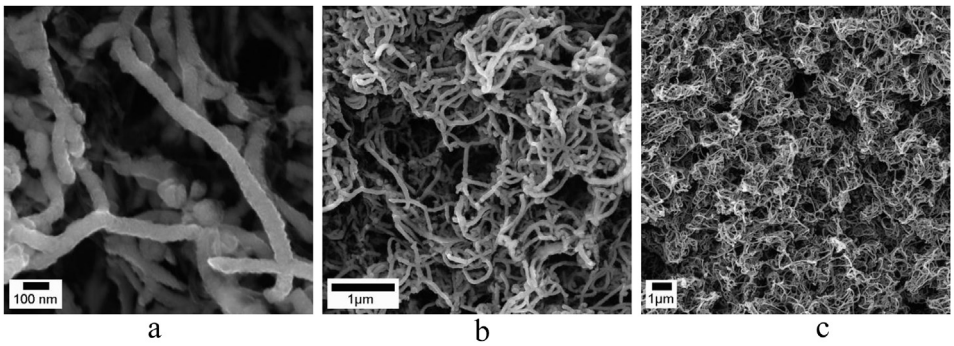

Fig. 13 – SEM images of CNT/Ni after electrolysis at (a) 200 K, (b) 50 K, (c) 15 K magnification.

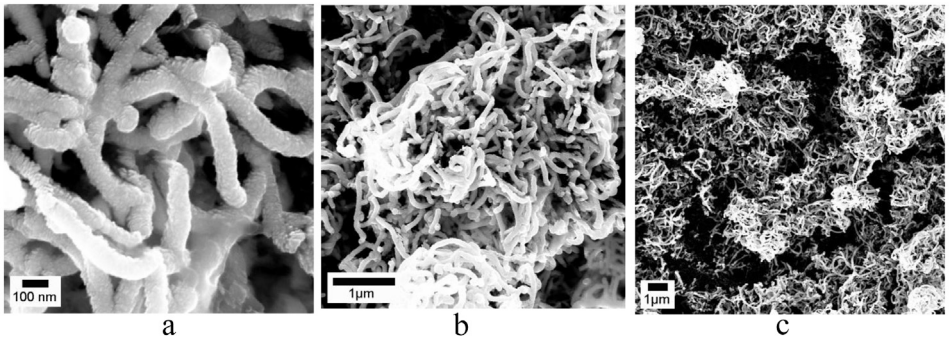

Fig. 14 – SEM images of CNT/Pd after electrolysis at (a) 200 K, (b) 50 K, (c) 15 K magnification.

Table 2 – CNTs/metal nanostructure diameters before and after 20 h of continuous electrolysis.

Sample	Before electrolysis avg. diameter (nm)	After electrolysis avg. diameter (nm)
CNTs/Co	60 ± 9	105 ± 23
CNTs/Ni	64 ± 6	65 ± 6
CNTs/Pd	77 ± 5	78 ± 7

different experimental conditions (lower catalyst loading, electrolyte pH and concentration), it can be noticed that our values are comparable with other solutions operating in neutral electrolyte [40–42]. As a secondary result, also our CNTs/Co and CNTs/Ni can be seen as promising HER catalyst. Even if the cathode performances are worst than CNTs/Pd and other reported systems, they show a low HER onset (250 mV)

Table 3 – XPS peaks of CNTs/metal nanostructures before and after 20 h continuous electrolysis.

Element/transition	Before electrolysis			After electrolysis			
	BE [eV]	FWHM [eV]	Area [counts eV]	BE [eV]	FWHM [eV]	Area [counts eV]	Peak assign.
Pd 3d 5/2	335.1	1.1	41790	334.9	1.1	45196	metallic Pd [30–32]
Pd 3d 3/2	340.4	1.1	27872	340.2	1.1	31872	metallic Pd [30–32]
Co 2p 3/2	777.9	1.3	12661	–	–	–	metallic Co [33,34]
Co 2p 3/2	780.6	2.0	75367	780.7	1.7	81044	Co(II) or Co(III) oxide [33,34]
Co 2p 3/2	785.8	7.4	57345	786.0	7.5	48235	satellite [33,34]
Co 2p 1/2	792.6	1.3	6204	–	–	–	metallic Co [33,34]
Co 2p 1/2	796.1	2.0	37223	796.0	1.7	39890	Co(II) or Co(III) oxide [33,34]
Co 2p 1/2	801.7	7.5	39547	802.3	7.5	29723	satellite [33,34]
Ni 2p 3/2	852.2	1.3	42342	852.2	1.3	2148	metallic Ni [33,35]
Ni 2p 3/2	854.9	2.3	59012	854.7	1.7	34080	Ni(II) oxide [33,35]
Ni 2p 3/2	860.2	6.2	62562	859.6	5.3	36691	satellite [33,35]
Ni 2p 1/2	869.7	1.4	19497	869.6	1.3	1074	metallic Ni [33,35]
Ni 2p 1/2	873.0	2.3	29541	872.8	1.7	16919	Ni(II) oxide [33,35]
Ni 2p 1/2	879.0	6.2	42943	878.7	5.3	26855	satellite [33,35]

red curve), the previously observed peak related to Ni(II) oxide (855.6 eV) and the satellite structure (860.0 eV) can still be identified. Peak related to metallic Ni (852.4 eV) is greatly reduced. This suggests a nearly complete oxidation of metallic Ni, without any change in the oxidation state of Ni(II) oxide (ratio between oxide to satellite signal is the same before and after electrolysis).

Conclusions

The good performances of our nanostructured electrodes can be attributed to a synergistic effect of the high surface area, thanks to the growth template conductive with CNTs, and the deposited catalytic material layer: output currents of catalytic materials alone, deposited on flat graphite, are one order of magnitude lower than catalytic layers deposited on nanotubes. Nevertheless, CNTs alone, with the high surface area but low catalytic properties, show very low output currents. Results show good performances of Co deposited on CNTs as electrodes for oxygen evolution. The catalytic activities of transition metal oxides is well known [6,38–41], and even if our deposition approach initially grows a metallic coating on nanotubes, the subsequent exposition to the atmosphere and oxidation cycle in electrochemical experiments quickly transform the metals into an appropriate oxide layer, as shown by XPS data. The onset over-potential required to start the reaction by electrodes described in this work ($\eta_{onse} < 200$ mV) lies in the same range, of other state of the art solutions [5,8,38]. On the other hand, registered current density values seem lower, but we have to take into account the and decent current densities. The undeniable advantage of using the same material (Co) as a bi-functional (HER and OER) catalyst is boosted by its low market price (Co price: about 2 orders of magnitude lower than Pd) [16]. Using the best performing HER and OER fabricated in this work, we successfully tested a working electrolyser, capable to output 4.5 mA cm^{-2} at a voltage of 1.50 V. This electrolyser is capable to output a stable, high current density for at least 20 h. As far as we know, few systems are capable to split water at this voltage [10,43]. Again, it is worth noticing that our system operates with a less concentrated electrolyte, and with a catalyst loading 1 to 2 orders of magnitude lower in respect to the solutions cited above. Summarizing, we successfully demonstrated that thermal evaporation of thin metal layers on CNTs bundles is a promising technique to fabricate efficient electrodes for water splitting. Moreover, we were able to assemble and test successfully a working electrolyser, capable to output high and stable current at the interesting low voltage of a single AA battery (1.50 V).

REFERENCES

[1] Carmo M, Fritz DL, Merge J, Stolten D. A comprehensive review on PEM water electrolysis. Int J Hydrogen Energy 2013;38:4901–34.

[2] Holladay JD, Hu J, King DL, Wang Y. An overview of hydrogen production technologies. Catal Today 2009;139:244–60.

[3] Ursua A, Gandia LM, Sanchis P. Hydrogen production from water electrolysis: current status and future trends. Proc IEEE 2012;100:410–26.

[4] Wang M, Wang Z, Gong X, Guo Z. The intensification technologies to water electrolysis for hydrogen production – a review. Renew Sustain Energy Rev 2014;29:573–88.
[5] Du S, Ren Z, Zhang J, Wu J, Xi W, Zhu J, et al. Co_3O_4 nanocrystal ink printed on carbon fiber paper as a large-area electrode for electrochemical water splitting. Chem Commun 2015;51:8066–9.
[6] Deng X, Tüysüz H. Cobalt-oxide-based materials as water oxidation catalyst: recent progress and challenges. ACS Catal 2014;4:3701–14.
[7] Osterloh FE, Parkinson BA. Recent developments in solar water-splitting photocatalysis. MRS Bull 2011;36:17–22.
[8] Zhao Y, Chen S, Sun B, Su D, Huang X, Liu H, et al. Graphene-Co_3O_4 nanocomposite as electrocatalyst with high performance for oxygen evolution reaction. Sci Rep 2015;5:7629.
[9] Dincă M, Surendranath Y, Nocera DG. Nickel-borate oxygen-evolving catalyst that functions under benign conditions. PNAS 2010;107:10337–41.
[10] Wang H, Lee H, Deng Y, Lu Z, Hsu P, Liu Y, et al. Bifunctional non-noble metal oxide nanoparticle electrocatalysts through lithium-induced conversion for overall water splitting. Nat Comm 2015;6:7261.
[11] Gong M, Zhou W, Tsai M, Zhou J, Guan M, Lin M, et al. Nanoscale nickel oxide/nickel heterostructures for active hydrogen evolution electrocatalysis. Nat Comm 2014;4:4695.
[12] Shao M. Palladium-based electrocatalysts for hydrogen oxidation and oxygen reduction reactions. J Power Source 2011;196:2433–44.
[13] Koenigsmanna C, Wong SS. One-dimensional noble metal electrocatalysts: a promising structural paradigm for direct methanol fuel cells. Energy Environ Sci 2011;4:1161–76.
[14] Grigoriev SA, Millet P, Fateev VN. Evaluation of carbon-supported Pt and Pd nano-particles for the hydrogen evolution reaction in PEM water electrolyser. J Power Source 2011;177:281–5.
[15] Kelly TG, Hunt ST, Esposito DV, Chen JG. Monolayer palladium supported on molybdenum and tungsten carbide substrates as low-cost hydrogen evolution reaction (HER) electrocatalysts. Int J Hydrogen Energy 2013;38:5638–44.
[16] www.infomine.com; www.monex.com (last access: September 2016).
[17] Mette K, Bergmann A, Tessonnier J, Hävecker M, Yao L, Ressler T, et al. Nanostructured manganese oxide supported on carbon nanotubes for electrocatalytic water splitting. ChemCatChem 2012;4:851–62.
[18] Yang Y, Fei H, Ruan G, Tour JM. Porous cobalt-based thin film as a bifunctional catalyst for hydrogen generation and oxygen generation. Adv Mater 2015;27:3175–80.
[19] Laursen AB, Vesborg PCK, Chorkendorf I. A high-porosity carbon molybdenum sulphide composite with enhanced electrochemical hydrogen evolution and stability. Chem Commun 2013;49:4965–7.
[20] Kong D, Wang H, Lu Z, Cui Y. $CoSe_2$ nano-particles grown on carbon fiber paper: an efficient and stable electrocatalyst for hydrogen evolution reaction. J Am Chem Soc 2014;136:4897–900.
[21] Suarez-Martinez I, Bittencourt C, Ke X, Felten A, Pireaux JJ, Ghijsen J, et al. Probing the interaction between gold nano-particles and oxygen functionalized carbon nanotubes. Carbon 2009;47:1549–54.
[22] Cargnello M, Grzelczak M, Rodriguez-Gonzalez B, Syrgiannis Z, Bakhmutsky K, La Parola V, et al. Multiwalled carbon nanotubes drive the activity of Metal@oxide core–shell catalysts in modular nanocomposites. J Am Chem Soc 2012;134:11760–6.
[23] Toma FM, Sartorel A, Iurlo M, Carraro M, Parisse P, Maccato C, et al. Efficient water oxidation at carbon nanotube–polyoxometalate electrocatalytic interfaces. Nat Chem 2010;2:826–31.
[24] Mazloumi M, Shadmehr S, Rangom Y, Nazar LF, Tang XS. Fabrication of three-dimensional carbon nanotube and metal oxide hybrid mesoporous architectures. ACS Nano 2013;7:4281–8.
[25] Eder D. Carbon nanotube–inorganic hybrids. Chem Rev 2010;110:1348–85.
[26] Hu CJ, Lin YH, Tang CW, Tsai MY, Hsu WK, Kuo HF. ZnO-coated carbon nanotubes: flexible piezoelectric generators. Adv Mater 2011;23:2941–5.
[27] Li XL, Li C, Zhang Y, Chu DP, Milne WI, Fan HJ. Atomic layer deposition of ZnO on multi-walled carbon nanotubes and its use for synthesis of CNT–ZnO heterostructures. Nanoscale Res Lett 2010;5:1836–40.
[28] Felten A, Ghijsen J, Pireau JJ, Drube W, Johnson RL, Liang D, et al. Electronic structure of Pd nano-particles on carbon nanotubes. Micron 2009;40:74–9.
[29] Bittencourt C, Hecq M, Felten A, Pireaux JJ, Ghijsen J, Felicissimo MP, et al. Platinum–carbon nanotube interaction. Chem Phys Lett 2008;462:260–4.
[30] Militello MC, Simko SJ. Elemental palladium by XPS. Surf Sci Spectra 1994;3:387–94.
[31] Militello MC, Simko SJ. Palladium oxide (PdO) by XPS. Surf Sci Spectra 1994;3:395–401.
[32] Adjizian JJ, De Marco P, Suarez-Martinez I, El Mel AA, Snyders R, Gengler RYN, et al. Platinum and palladium on carbon nanotubes: experimental and theoretical studies. Chem Phys Lett 2013;571:44–8.
[33] McIntyre NS, Cook MG. X-ray photoelectron studies on some oxides and hydroxides of cobalt, nickel, and copper. Anal Chem 1975;47:2208–13.
[34] Armelao L, Barreca D, Gross S, Tondello E. Sol-gel and CVD Co_3O_4 thin films characterized by XPS. Surf Sci Spectra 2001;8:14–23.
[35] Mansour AN, Melendres CA. Characterization of $Ni_2O_3 \cdot 6H_2O$ by XPS. Surf Sci Spectra 1994;3:263–70.
[36] Duncan H, Lasia A. Separation of hydrogen adsorption and absorption on Pd thin films. Electrochim Acta 2008;53:6845–50.
[37] Kedzierzawski P, Mikołajczuk A, Borodziński A, Mierzwa B, Stobiński L. Novel metastable Pd-Ru catalysts for electrooxidation of formic acid. ECS Trans 2010;28:23–31.
[38] Lu X, Zhao C. Electrodeposition of hierarchically structured three-dimensional nickel–iron electrodes for efficient oxygen evolution at high current densities. Nat Commun 2015;6:6616.
[39] Jin H, Wang J, Su D, Wei Z, Pang Z, Wang Y. In situ cobalt–cobalt oxide/N-doped carbon hybrids as superior bifunctional electrocatalysts for hydrogen and oxygen evolution. J Am Chem Soc 2015;137:2688–94.
[40] Esswein AJ, Surendranath Y, Reece SY, Nocera DG. Highly active cobalt phosphate and borate based oxygen evolving catalysts operating in neutral and natural waters. Energy Environ Sci 2001;4:499–504.
[41] Kanan MW, Nocera DG. In situ formation of an oxygen-evolving catalyst in neutral water containing phosphate and Co2+. Science 2008;321:1072–5.
[42] Wu Y, Chen M, Han Y, Luo H, Su X, Zhang M-T, et al. Fast ans simple preparation of iron-based thin films as highly efficient water-oxidation catalysts in neutral aqueous solutions. Angew Chem Int Ed 2015;54:1–7.
[43] Ma W, Ma R, Wang C, Liang J, Liu X, Zhou K, et al. A superlattice of alternately stacked Ni–Fe hydroxide nanosheets and graphene for efficient splitting of water. ACS Nano 2015;9:1977–84.